Local structural disorder and its influence on the average global structure and polar properties in $Na_{0.5}Bi_{0.5}TiO_3$

Badari Narayana Rao,[1] Ranjan Datta,[2] S. Selva Chandrashekaran,[3] Dileep K. Mishra,[4] Vasant Sathe,[4] Anatoliy Senyshyn,[5] and Rajeev Ranjan[1,*]

[1]*Department of Materials Engineering, Indian Institute of Science, Bangalore 560012, India*

[2]*International Centre for Materials Science, Chemistry and Physics of Materials Unit, Jawaharlal Nehru Centre for Advanced Scientific Research, Jakkur P.O., Bangalore 560064, India*

[3]*Functional Materials Division, CSIR Central Electrochemical Research Institute, Karaikudi 630001, India*

[4]*UGC-DAE Consortium for Scientific Research, University Campus, Khandwa Road, Indore 452017, India*

[5]*Forschungs-Neutronenquelle Heinz Maier-Leibnitz (FRM II), Technische Universität München, Lichtenbergstrasse 1, D-85747 Garching b. München, Germany*

(Received 4 September 2013; revised manuscript received 10 November 2013; published 10 December 2013)

$Na_{0.5}Bi_{0.5}TiO_3$ (NBT) and its derivatives have prompted a great surge in interest owing to their potential as lead-free piezoelectrics. In spite of five decades since its discovery, there is still a lack of clarity on crucial issues such as the origin of significant dielectric relaxation at room temperature, structural factors influencing its depoling, and the status of the recently proposed monoclinic (Cc) structure vis-à-vis the nanosized structural heterogeneities. In this work, these issues are resolved by comparative analysis of local and global structures on poled and unpoled NBT specimens using electron, x-ray, and neutron diffraction in conjunction with first-principles calculation, dielectric, ferroelectric, and piezoelectric measurements. The reported global monoclinic (Cc) distortion is shown not to correspond to the thermodynamic equilibrium state at room temperature. The global monoclinic like appearance rather owes its origin to the presence of local structural and strain heterogeneities. Poling removes the structural inhomogeneities and establishes a long-range rhombohedral distortion. In the process the system gets irreversibly transformed from a nonergodic relaxor to a normal ferroelectric state. The thermal depoling is shown to be associated with the onset of incompatible in-phase tilted octahedral regions in the field-stabilized long range rhombohedral distortion.

DOI: 10.1103/PhysRevB.88.224103 PACS number(s): 77.80.−e, 77.22.−d, 77.80.Jk, 77.84.Cg

I. INTRODUCTION

Lead zirconate titanate (PZT)-based piezoelectric ceramics are widely being used in electronic devices due to their superior piezoelectric properties. However, lead oxide is toxic and volatile at processing temperatures and causes environmental pollution when these materials are disposed. As a result, there is a pressing need to substitute PZT with lead-free piezoelectric ceramics. Bismuth-based perovskite compounds are among the promising class of materials in this regard as the electronic configuration of Bi^{3+} is same as that of Pb^{2+} and hence is expected to impart similar properties as that in lead-based ceramics. $Na_{0.5}Bi_{0.5}TiO_3$ (NBT) is one such interesting compound with A-site disorder, which was first discovered in 1961 by Smolenskii *et al.*[1] Suitable chemical modification of NBT has been anticipated to yield a desirable lead-free piezoelectric material. A tremendous surge in research on $Na_{0.5}Bi_{0.5}TiO_3$ and its derivatives after the discovery of high strain that exceed those achieved by PZT has been witnessed in the past few years.[2] Interestingly, though a great volume of literature reporting the structure-property correlations of solid solutions of NBT with $BaTiO_3$, $KNaNbO_3$, and $K_{1/2}Bi_{1/2}TiO_3$ exists,[3–22] a clear understanding of their structural aspects still remain incomplete. The most important reason is related to the fact that the true structure and phase-transition behavior of the parent compound NBT has eluded clarity even five decades after its discovery.

Until recently, NBT was considered to possess rhombohedral perovskite ($R3c$) structure.[23] However, many groups have reported the occurrence of local disordered regions in NBT by neutron diffuse scattering,[24] x-ray diffuse scattering,[25] x-ray absorption fine structure (XAFS),[26] etc. These disorders have been attributed to small perpendicular displacements of Bi^{+3} cations away from the polar $\langle 111\rangle_c$ direction in order to improve its coordination environment. Bond-valence calculations have shown that Bi^{+3} is heavily under bonded in the average rhombohedral structure.[23] Questioning the traditionally accepted $R3c$ structure, Gorfman and Thomas[27] suggested an average monoclinic (Cc) structure at room temperature using high resolution single crystal x-ray diffraction (XRD) study. Subsequent experiments using optical birefringence[28] and synchrotron x-ray powder diffraction[29] have affirmed the global monoclinic distortion. Electron diffraction studies, on the other hand, have suggested another aspect of departure from pure rhombohedral symmetry on a local length scale.[30–32] These studies have revealed additional weak superlattice reflections of the odd-odd-even $\frac{1}{2}\{ooe\}_c$ (notation in accordance with Glazer's scheme[33,34]) type along with diffuse rodlike scattering,[33] indicating a presence of thin sheets of localized in-phase (+) tilted octahedral regions. These tilts are incompatible with both $R3c$ (tilt system: $a^-a^-a^-$) and the currently suggested Cc (tilt system $a^-a^-c^-$) structures. Recently, Ma *et al.*[35] used the difference in probability for observing $\frac{1}{2}\{ooo\}_c$ spots in $R3c$ and Cc structures to prove the room temperature structure of NBT to be Cc. However, they have not commented on the presence of the in-phase tilt component that has been observed by other groups. It may be noted that the superlattice reflections characteristic of

the in-phase tilt have never been captured in bulk diffraction techniques, such as x-ray or neutron diffraction at room temperature, thereby suggesting their extremely small size as compared to the coherence length of the x-ray/neutrons used. Rao and Ranjan[36] have recently demonstrated that the structure of NBT becomes perfectly rhombohedral (space group $R3c$) once it is electrically poled. Subsequently, Rao *et al.*[37] argued in favor of the $R3c + Cc$ phase coexistence model for the unpoled state. The relative volume fraction of the two phases was found to be highly susceptible to thermal treatment, application of mechanical stress, or electric field.

Further, there is also a lack of unanimity on the temperature evolution of structural and polar ordering in NBT. The traditional view of the structural transitions is summarized in the work of Jones and Thomas,[23] who proposed the following phase transition sequence:

$$R3c \overset{250^{0c}}{\Leftrightarrow} R3c{+}P4bm \overset{397^{0c}}{\Leftrightarrow} P4bm \overset{540^{0c}}{\Leftrightarrow} Pm3m.$$

Subsequent experiments have verified this sequence of structural transition[38] (with recent reports replacing the $R3c$ by Cc). Optical isotropization around 300 °C has also been reported for NBT,[28,38–40] which could either be attributable to the presence of an actual cubic phase at that temperature or to the existence of optically small but anisotropic domains with random orientation of their optical indicatrices. The relative permittivity of NBT shows a weak anomaly (as a shoulder) at ∼200 °C and a peak at ∼325 °C (Ref. 41). Though the system is known to significantly depolarize above ∼200 °C, earlier reports have set the Curie point at ∼325 °C. So far no distinct structural transformation has been reported at the depolarization temperature. Dorcet *et al.*[42–44] have reported emergence of octahedral tilt modulation in the temperature range of 200–290 °C and related it to the relaxor and antiferroelectric behavior of NBT in this temperature region. In a recent high temperature structural study using high resolution synchrotron x-ray powder diffraction, Aksel *et al.*[45] reported the tetragonal phase in the temperature range 280–510 °C and considered the monoclinic (Cc) + cubic ($Pm3m$) model below 280 °C. The cubic phase was included to account for the misfit regions in the diffraction pattern attributed to the presence of local disorders in the system, the origin of which has not been discussed. Very recently, a phase transition into the tetragonal phase involving bifurcated polarization rotation of Bi^{3+} has also been reported using neutron pair distribution analysis.[46]

From the above, it seems obvious that although several studies have been reported on NBT, there is still a lack of coherent understanding with regard to its structure and dielectric/ferroelectric behavior. Some questions that deserve serious attention and have direct bearing with regard to the understanding of the piezoelectric properties of NBT-derived systems include the following. (i) Is Cc a genuine thermodynamic equilibrium phase? (ii) Is there a relationship between the average monoclinic distortion and the nanosized structural heterogeneities? (iii) What factors influence the coherence length and the volume fraction of the local structural heterogeneities? and (iv) What is the relationship between the relaxor/normal ferroelectric behavior and the perceived structures at different length scales? The answers to these questions require a way to relate the dielectric and the ferroelectric properties to the structural features observed at all pertinent length scales. We have tackled this complex issue through a comparative study on poled and unpoled NBT specimens using a series of techniques: first-principles computation, electron diffraction, high temperature x-ray, neutron diffraction, and Raman spectroscopy. The study was also complemented by a self-consistent set of dielectric and polarization measurements. The results indicate that the reported global monoclinic (Cc) structure does not correspond to a thermodynamic equilibrium state. A one-to-one correlation between the coherence length of localized $a^0a^0c^+$ tilts and the monocliniclike appearance in the global diffraction pattern was found. The electric field drastically reduces the coherence length of the in-phase octahedral tilt and also the strain in the average lattice. In the absence of both these interrelated features, the system reveals its global rhombohedral ($R3c$) symmetry and a normal ferroelectric state (instead of a relaxor ferroelectric state).

II. EXPERIMENTAL SECTION

A. Method

NBT ceramics were prepared by the conventional solid state route. Dried oxides of high purity Bi_2O_3, Na_2CO_3, and TiO_2 were used as raw materials. Stoichiometric amounts of the oxides were mixed in a planetary ball mill for 10 h, with acetone as the mixing medium using zirconia bowls and balls. After drying, the mixed powders were calcined at 900 °C for 2 h in an alumina crucible. The calcined powders were then mixed with 2% polyvinyl alcohol (PVA), pressed into pellets by uniaxial pressing at 100 MPa, and then compacted by cold isostatic pressing at 300 MPa. These pellets were then sintered in air at 1140 °C for 3 h. Density measurements carried out using Archimedes' principle showed the pellet to have a density of 98.5% of the theoretical density. Poling was carried out at room temperature in silicone oil by applying a dc electrical field of 70 kV/cm for 10 min on the sintered pellets. Powder XRD patterns at room temperature and high temperature were collected from a Bruker powder diffractometer (model D8 Advance) using a Cu $K\alpha$ x-ray source and nickel filter. Room temperature and high temperature neutron powder diffraction data were collected using a wavelength of 1.548183 Å on the Structure Powder Diffractometer (SPODI) at the FRM II neutron reactor (Germany).[47] The powders for the high temperature scans were taken in a niobium container; hence, the patterns contain additional niobium peaks. Rietveld refinement was carried out using the FULLPROF package (2000; Ref. 48). The refined parameters include 2θ-zero, background fitted by linear interpolation, lattice parameter, atomic coordinates, thermal displacement parameters, and the pseudo-Voigt profile shape parameters. A precision Premier II tester (Radiant Technologies, Inc.) was used to obtain the polarization-electric field (P-E) loop measurements. The piezoelectric coefficient d_{33} was measured using a Berlincourt meter from Piezotest (model PM300). The high temperature Raman measurements were carried out in the backscattering geometry using an Ar + laser excitation source at 488 nm attached with a LABRAM HR-800 spectrometer and a charge-coupled device (CCD) detector. The measurements were carried out on a pellet loaded

in a Linkam (UK) temperature-variation cell with a stability of 0.1 °C. The dielectric measurements were carried out using a Novocontrol Alpha-A impedance analyzer. An FEI Titan Cubed (80–300 kV) was used to carry out the transmission electron microscopy (TEM) characterization. All the high temperature experiments were carried out on the poled NBT sample, and measurements were made in both the heating and cooling cycles. As the structure resembles that of the unpoled state after heating to a sufficiently high temperature, for all practical purposes the cooling data can be considered as that of the unpoled sample.

B. Computational details

First-principles computation, based on density functional theory and implemented in the Vienna *Ab initio* Simulation Package (VASP),[49] was performed to study the structural stability of the Cc phase with respect to $R3c$ in NBT. Valence electron wave functions of all the atoms are conveniently described by the projector-augmented wave (PAW) functional.[50] The exchange correlation part of total energy was corrected by generalized gradient approximations (GGA).[51] For a good convergence of ground state energy, the high kinetic cutoff energy of 500 eV was set as the plane wave basis. The Brillouin zone of the periodic cell was sampled by the Monkhorst-Pack method with a $6 \times 6 \times 2$ and $2 \times 6 \times 6$ k-point mesh for $R3c$ and Cc structures, respectively. For partial occupancies of the orbital, the Gaussian-smearing scheme with a finite electronic temperature of 0.1 eV was set. Using self-consistent calculation, both ionic and electronic relaxations were alternatively performed until the energy difference of two successive ionic steps and the force constant of ions converged below 0.1 meV and 1 meV/Å, respectively.

III. RESULTS

A. Relative stability of the $R3c$ and Cc structures—first-principles study

While examining the status of the recently proposed monoclinic (Cc) structure of NBT vis-à-vis the traditional rhombohedral ($R3c$) phase, a comparative study was carried out using first-principles computation. The rhombohedral (in the hexagonal setting) and monoclinic unit cell consists of six and four formula units of NBT, respectively (Fig. 1). In a recent paper by Ma *et al.*,[52] first-principles calculations of NBT were reported by considering $NaTiO_3$- and $BiTiO_3$-ordered layers in the $[111]_{pc}$ and $[001]_{pc}$ pseudocubic directions. The authors reported that for any given structural distortion, the model with $[111]_c$ ordering gave lower energy as compared to that with $[001]_c$ ordering. Further, among the four noncubic distortions, $R3c$, $P4bm$, $P4mm$, and $R3m$, the lowest energy was reported for the $R3c$ model. More recently, Niranjan *et al.*[53] showed that the $R3c$ model with $[111]_c$ ordering of Na and Bi could reasonably reproduce the experimental values of atomic coordinates, lattice parameters, and the frequencies of the transverse optical (TO) and longitudinal optical (LO) modes. These studies suggest that although the assumed ordered structural model does not actually represent the experimental situation, it is not a bad model when it comes to predicting properties. In view of this, we also considered the

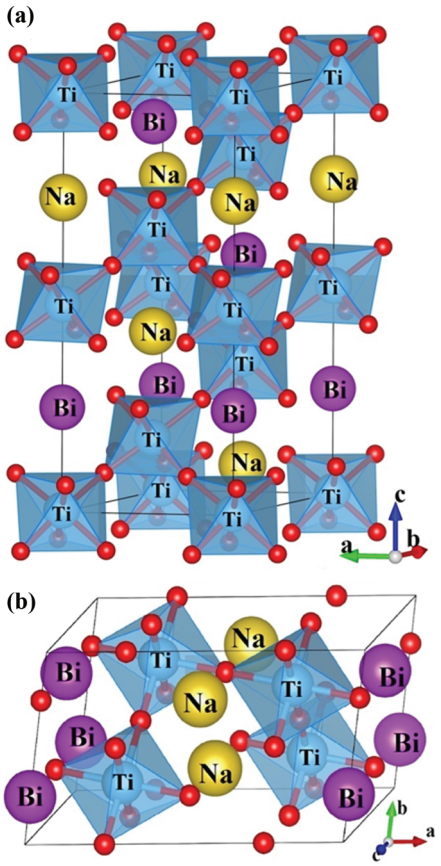

FIG. 1. (Color online) Crystal structure models of (a) rhombohedral $R3c$ (hexagonal setting) and (b) monoclinic Cc phases considered in the first-principles calculations, drawn using the VESTA package.

$[111]_c$-ordered Na and Bi layers for determining the relative stability of the $R3c$ and Cc distortions. In the hexagonal setting of the $R3c$ structure, the $[111]_c$ direction is parallel to the c axis. In the Cc structure, this direction corresponds to the [101] direction of the monoclinic unit cell. The initial cell parameters of rhombohedral ($R3c$ space group) and monoclinic (Cc space group) structures were taken from the experimental results[37] and allowed to relax self-consistently through ground state energy configuration. The optimized lattice parameters are in good agreement with experimental values (98–100%; Table I). Interestingly, the minimum energy of the Cc structure turns out to be 106 meV/formula units higher than the minimum energy of $R3c$ structure (Fig. 2). This difference is comparable to the

TABLE I. The lattice parameters of the monoclinic and rhombohedral structures calculated from first-principles computation. The experimental parameters are also given for comparison.

	Experiment		Theory	
Lattice parameters	$R3c$	Cc	$R3c$	Cc
a (Å)	5.484	9.5196	5.475	9.585
b (Å)	5.484	5.4798	5.475	5.507
c (Å)	13.548	5.5114	13.556	5.542
β (deg.)	–	125.278	–	125.43

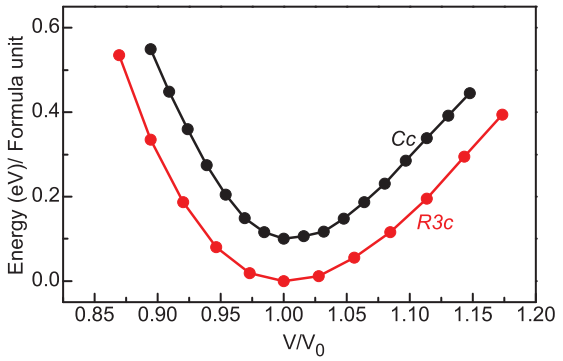

FIG. 2. (Color online) Volume dependence of the relative energies per formula unit of the monoclinic and the rhombohedral phases. V_0 represents the equilibrium volume.

values reported by Ma *et al.*, who showed that with respect to $R3c$, the energy per formula unit of $P4bm$, $P4mm$, and $R3m$ structures are higher by 98, 93, and 133 meV, respectively.[52] Because the E-V curves of the Cc and the $R3c$ phases do not intersect for the compressed and expanded volumes, the possibility of pressure-induced Cc-$R3c$ transition is also less likely. Hence, within the chosen chemically ordered structural framework, first-principles results suggest that a global Cc phase is energetically less stable compared to the global $R3c$ phase. In the sections that follow, we present experimental evidences to show that the global monoclinic distortion observed in high resolution x-ray/neutron diffraction patterns does not correspond to an equilibrium state but is intimately linked to the presence of nanosized structural heterogeneity and strain in the average lattice.

B. Field-induced disappearance of the average monoclinic distortion

Figure 3 shows the Rietveld-fitted room temperature neutron diffraction patterns with the rhombohedral $R3c$ structural model on poled and unpoled NBT specimens. For the unpoled specimen, it is evident from the inset that the fits are not satisfactory at higher angles. This misfit can be attributed to the disorder and the average monoclinic distortion reported in recent years.[27,29] On the contrary, the $R3c$ model fits the entire diffraction pattern of the poled specimen perfectly well. This corroborates the results reported earlier from an XRD study[36] and confirms the disappearance of the monocliniclike average distortion after application of the poling field. The refined structural parameters obtained from the neutron diffraction data of the poled specimen are given in Table II. If the monoclinic structure is considered to be genuine, this result would imply a field-driven monoclinic to rhombohedral irreversible structural phase transition.

C. Field-induced disappearance of the localized in-phase tilt

The different aspects of the deviation from the global rhombohedral structure captured by the x-rays and electron and neutron scattering studies most likely arise from the same nanosized structural heterogeneity. In order to establish a one-to-one correlation between the local structural heterogeneity and the monocliniclike global distortion, a comparative

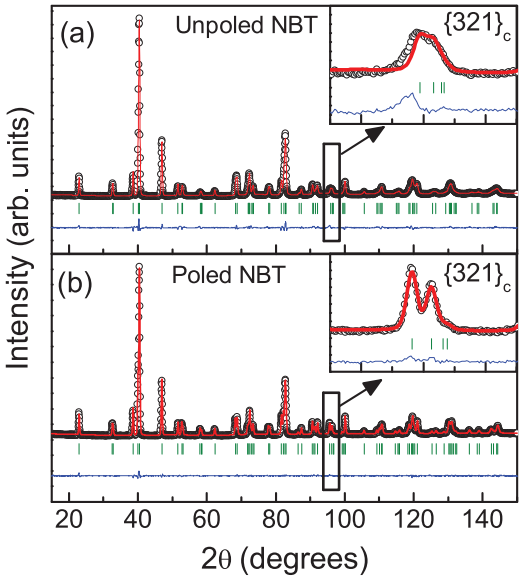

FIG. 3. (Color online) Rietveld refinement fit of (a) unpoled NBT powder and (b) poled NBT powder using neutron diffraction data with the $R3c$ structural model. Insets show the zoomed plot of the $\{321\}_c$ Bragg peak.

electron diffraction study of both the poled and the unpoled specimen were carried out. Figure 4 displays the $[111]_c$ and $[310]_c$ zone TEM diffraction patterns for unpoled and poled NBT. In conformity with the reports in the past, we can see evidence of in-phase octahedral tilt in the form of

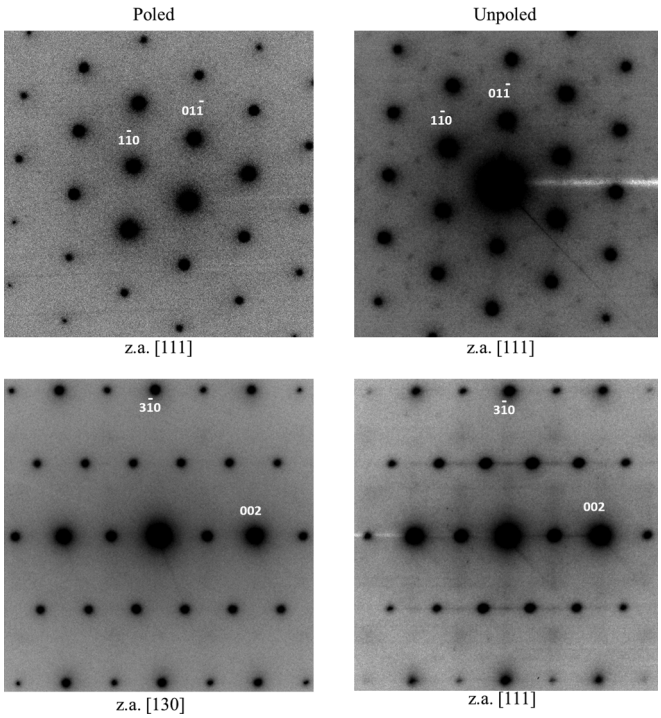

FIG. 4. $\{111\}_c$ and $\{310\}_c$ zone TEM diffraction patterns of poled and unpoled samples. Poled samples shows perfect rhombohedral features, whereas unpoled samples features extra superlattice spots corresponding to $\frac{1}{2}\{ooe\}_c$-type reflections ($[111]_c$ pattern) and traces of $\{100\}_c$ sheets ($[130]_c$ pattern).

TABLE II. Structural parameters of poled NBT obtained by Rietveld analysis of neutron powder diffraction data. U^{ij} represents the anisotropic displacement parameters.

Atom	x	Y	z		
Na/Bi	0	0	0.27643 (10)		
Ti	0	0	0.01077 (16)		
O	0.12121 (15)	0.3384 (2)	0.08330*		
	$U^{11} = U^{22}$	U^{33}	U^{12}	U^{13}	U^{23}
Na/Bi	0.0261 (6)	0.0213 (9)	0.0130 (6)	0	0
Ti	0.0067 (7)	0.0082 (10)	0.0033 (7)	0	0
O	0.0114 (5)	0.0213 (3)	0.0039 (5)	−0.0032 (4)	−0.0103 (3)

$a = 5.47906$ (4) Å, $c = 13.56102$ (16) Å
Residual Factors: $R_{wp} = 2.97$ $\chi^2 = 1.85$

*O(z) was fixed to deal with the floating origin.

$\frac{1}{2}\{ooe\}_c$-type weak superlattice spots, which are inconsistent with the $R3c$ structure. The diffuse streaks running along the $[100]_c$ direction in the $[310]_c$ zone pattern further confirm the disorder to be present as planar defects. Interestingly, the $\frac{1}{2}\{ooe\}_c$ superlattice spots and the diffuse streaks are not seen in the diffraction pattern of the poled sample. A significant reduction in the strain contrast can also be easily noticed in the high resolution TEM (HRTEM) image of the poled specimen (Fig. 5). The fast Fourier transform (FFT) of the high resolution images from the poled sample is mostly

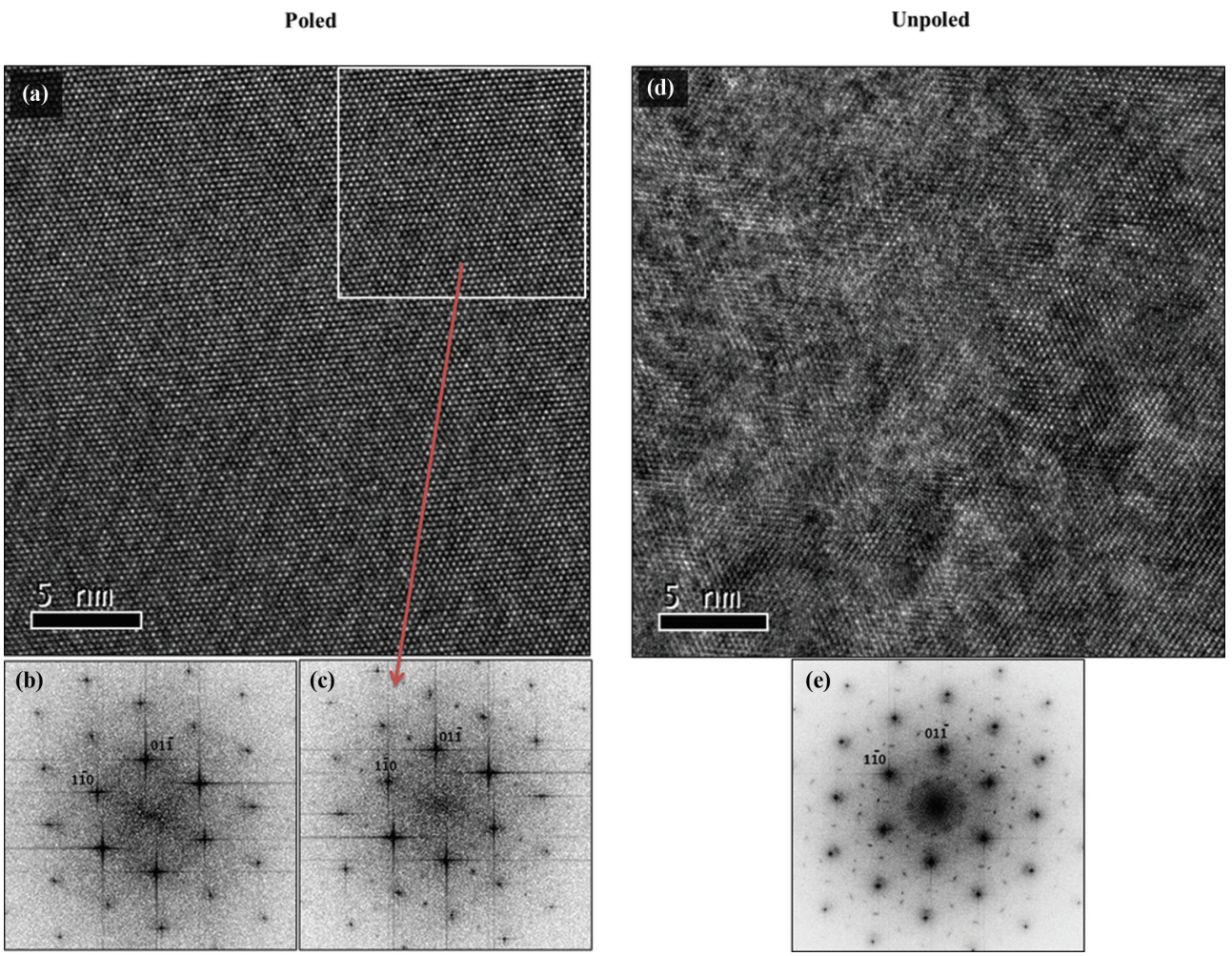

FIG. 5. (Color online) (a) Raw HRTEM image along $[111]_c$ orientation obtained from a poled NBT specimen. (b) FFT of the HR image in (a) from the majority of the areas. (c) FFT of a selected area (shown as white square) from (a), which shows additional faint superlattice spots similar to the unpoled sample. (d) Raw HRTEM image along $[111]_c$ orientation obtained from unpoled NBT sample. (e) Corresponding FFT of the HR image in (d), showing $\frac{1}{2}\{ooe\}_c$ superlattice reflections.

devoid of $\frac{1}{2}\{ooe\}_c$ superlattice spots [Fig. 5(b)]. However, some localized regions still show these superlattice spots [Fig. 5(c)], whose intensity is very low when compared with that of the unpoled sample [Fig. 5(e)]. This situation, though a minor one, might be due to additional disorders created during the unavoidable mechanical grinding and ion milling involved during the TEM sample preparation process. It may be noted that the $\frac{1}{2}\{ooe\}_c$ spots are not seen in the conventional TEM diffraction patterns of the poled sample, where the selected area aperture selects about a half-micron square sample area, compared to considerably smaller areas sampled from HRTEM images. These results suggest that the poled sample exhibits drastically reduced regions of in-phase octahedral tilts as compared to the unpoled specimen. The simultaneous disappearance of the monoclinic distortion (in bulk XRD), the in-phase tilted regions (in electron diffraction), and the heterogeneous lattice strain on poling proves one-to-one correspondence between localized in-phase tilted octahedral regions and the perceived monoclinic distortion on a global scale.

D. Field-induced transformation of the relaxor state to a normal ferroelectric state

Figure 6 shows the variation of the *P*-*E* hysteresis loop at different values of maximum applied field (E_{max}). The measurement was carried out on an initially unpoled NBT pellet at a constant frequency of 1 Hz. In each subsequent cycle, E_{max} was incremented until a saturated hysteresis loop was obtained. Once a saturated loop was obtained, the E_{max} in the subsequent cycles were continuously decreased. As shown in Fig. 6, though the first saturated loop was observed only at E_{max} of 64 kV/cm, it was relatively easy to obtain saturation at a lower E_{max} once polarization saturation was achieved [Fig. 6(c)]. Since electron diffraction study has already shown that poling drastically reduces the coherence length

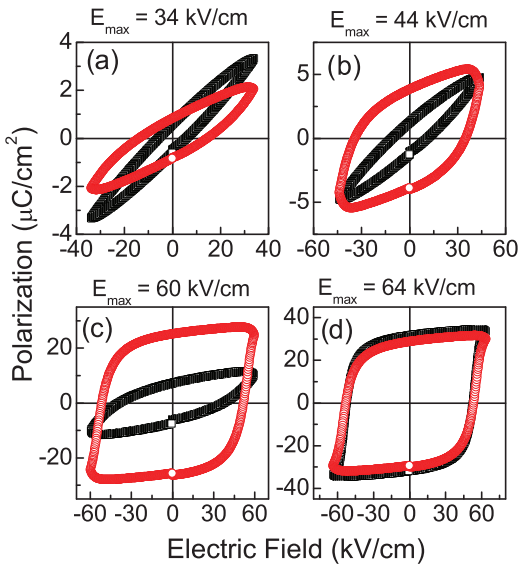

FIG. 6. (Color online) The trend of the *P*-*E* loops obtained from an initially unpoled NBT pellet at varying E_{max}. The black loop shows the trend during increasing E_{max}, (squares), whereas the red loop shows the trend during decreasing E_{max} (circles).

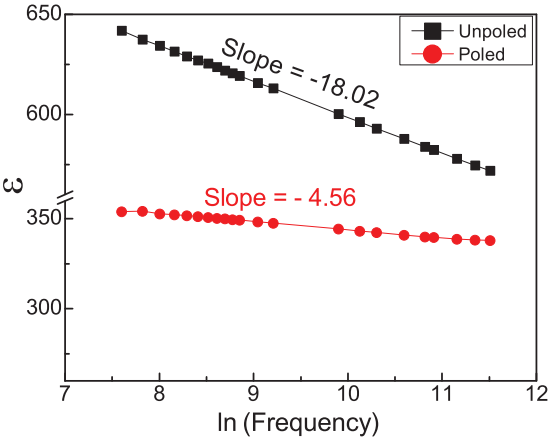

FIG. 7. (Color online) Frequency vs relative permittivity plot for the poled and unpoled sample at room temperature.

of the in-phase tilted region and makes the average lattice homogeneous, it appears that the higher field required initially for obtaining polarization saturation is related to overcoming the hindrance posed by these local structural heterogeneities. It must also be noted that these comparisons were made at one particular frequency. Decreasing the frequency would cause the polarization saturation during increasing E_{max} to occur at a lower field as the domains get more time to align in the field direction. In this context, it may be noted that poling an NBT sample for sufficient time, even at 40 kV/cm, was enough to obtain the global *R*3*c* distortion, and the d_{33} value obtained was close to that obtained at higher poling fields.[37]

Another notable difference between the poled and unpoled NBT specimen was found in the degree of their dielectric dispersions. As shown in Fig. 7, the plot of dielectric permittivity vs log frequency shows a linear trend. The slope of the linear plot can be taken as a measure of the degree of dielectric dispersion. The slope in the unpoled state is about 3.5 times larger than that in the poled state. The considerably enhanced relaxation in the unpoled state is due to lack of long-range polarization, which in turn, as shown above, is due to the lack of long range structural coherence. Vakhrushev *et al.*[54] have reported average size of the polar domains to be of the order of ∼11 nm at room temperature. Levin and Reaney[32] have argued about structural inhomogeneities at two different length scales, i.e. 1–3 nm of the tetragonal ($a^0a^0c^+$) regions embedded in pseudorhombohedral twin domains of 10–40 nm thickness. A modulated domain structure of real space period of ∼ 4 nm has been suggested by Thomas *et al.*[55] Balagurov *et al.*[24] have argued about incommensurate modulation of the *R*3*c* phase along the fourfold axis of the precursor tetragonal phase. While we have shown that the coherence length of in-phase tilted octahedral regions is dramatically reduced after poling, we also anticipate that poling would drastically reduce the diffuse scattering signal in x-ray/neutron scattering studies and also that the incommensurate modulation[24] would disappear.

E. Depoling and normal to relaxor ferroelectric transition

The inset in Fig. 8(a) shows the variation of remnant polarization with temperature, which gives an insight into

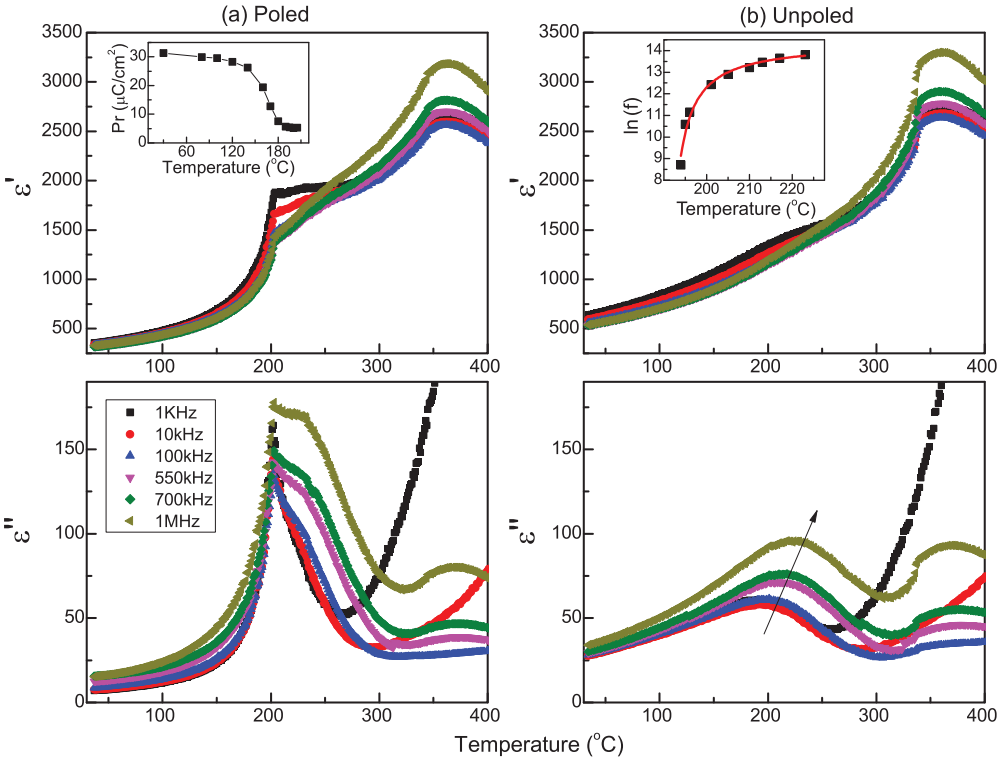

FIG. 8. (Color online) Temperature variation of the real and imaginary parts of relative permittivities of (a) poled and (b) unpoled NBT. Inset in (a) shows variation of remnant polarization as a function of temperature. Inset in (b) shows the Vögel-Fulcher fitting of frequency vs T_m, the temperature of maximum in imaginary part of dielectric permittivity.

the depoling behavior of NBT. The depoling seems to start above 150 °C and ends at 190 °C. The temperature of 190 °C is generally treated as the depolarization temperature of NBT. While at the visual level, the temperature dependence of polarization observed [Fig. 8(a)] is typical of any ferroelectric material; it will be shown in Sec. III G that the onset of depoling at 150 °C is due to a subtle but distinct structural change. Figures 8(a) and 8(b) show the temperature variation of the real and imaginary parts of the relative permittivity of the poled and unpoled NBT at different frequencies. The real and imaginary parts in the poled sample show sharp anomaly at 200 °C, suggesting a phase transition. Above 200 °C, both quantities begin to display dielectric relaxation. In view of this, the anomaly at 200 °C can also be termed as the normal to relaxor ferroelectric transition ($T_{F\text{-}R}$). In contrast, the unpoled sample merely shows a weak shoulder around this temperature in the real part and relaxational peaks characteristic of a relaxor ferroelectric in the imaginary part. A Vögel-Fulcher analysis[56,57] using the data of the imaginary part of the unpoled specimen [inset of Fig. 8(b)] gives the freezing temperature of the polar clusters (T_f) to be 190 °C. This is about 10 °C less than the normal to relaxor ferroelectric transition temperature ($T_{F\text{-}R}$) exhibited by the poled specimen. A similar observation has been made earlier for NBT substituted with 6 mol% $BaTiO_3$, where depolarization has been explained in terms of a two-stage process involving major randomization of the domains followed by breaking of the domains into nanoregions.[58]

F. Temperature-induced structural transformations: Raman studies

In the past, high temperature Raman spectra of NBT have been analyzed by different groups.[59–62] The results suggest a broad distribution of local structural distortions in the different phases of NBT. Luo *et al.*[62] have reported the persistence of local polarization due to asymmetric Ti-O vibrations well above T_{max} (∼325 °C), the temperature corresponding to maxima in the relative permittivity of NBT. Low frequency modes corresponding to the *A*-site bonds are regarded as a main source for relaxor features in NBT. These modes are reported to exhibit anomalies in their intensity variation in the vicinity of the rhombohedral-tetragonal transition (300 °C).[60] However, the diffuse nature of the modes with considerable overlapping made it difficult to precisely determine the transition temperatures. Here, we compare the temperature dependence of the Raman spectra obtained from the poled and unpoled sample. Figure 9(a) displays the temperature evolution of the Raman spectra of the poled NBT pellet during the heating and cooling cycle. The cooling data can be treated as that of the unpoled sample since the specimen loses its poling-related memory after heating into the paraelectric state. The observed room temperature spectrum of our unpoled sample is consistent with the previous reports.[15,20,63] The dashed lines are drawn as a guide for the eye to show peak shifts. The room temperature modes of NBT are mainly centered in three regions: (A) 100–200 cm^{-1}, (B) 200–400 cm^{-1}, and (C) 400–650 cm^{-1}. Following Kreisel *et al.*,[20,63] the

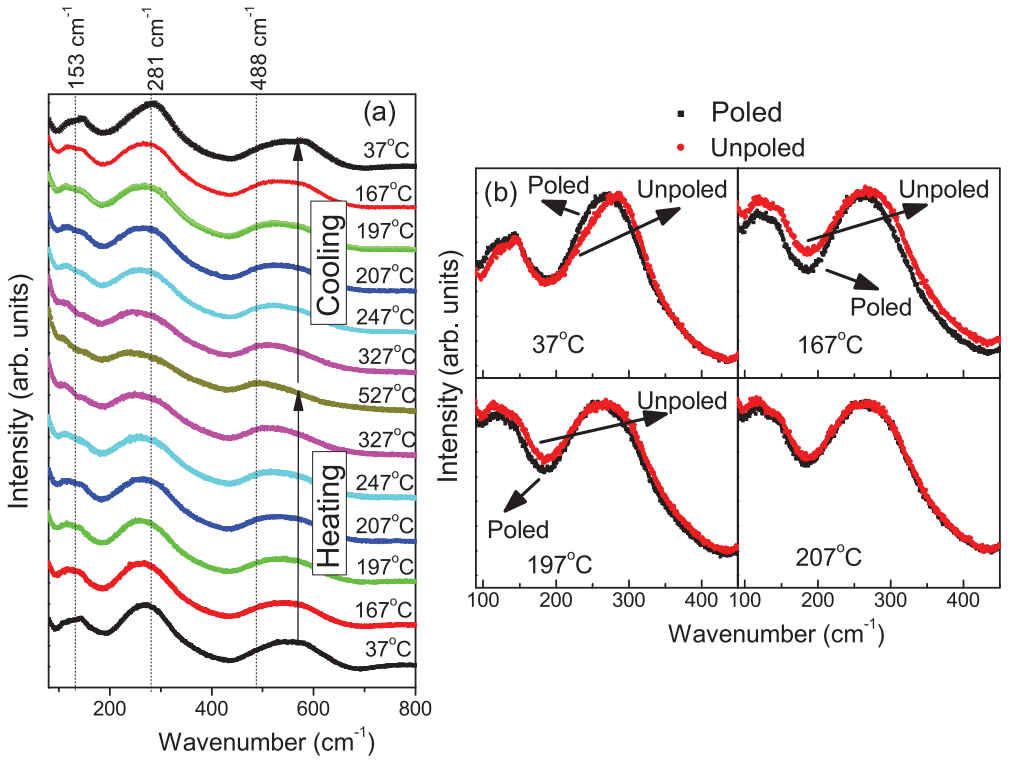

FIG. 9. (Color online) (a) The temperature dependence of the Raman spectra for the poled sample heated up to a temperature of 527 °C and then cooled to room temperature. The cooling data can be considered as the data for the unpoled sample. (b) Comparison of the selected Raman modes at particular temperatures for the poled and unpoled sample.

mode in region A is associated with Na-O vibration, the broad band in region B is dominated by Ti-O vibration, and the modes in region C are dominated mainly by vibrations involving oxygen displacements. With increase in temperature all of the modes become broad. The modes in region A gradually weaken and disappear above 300 °C. Figure 9(b) compares the mode in region B of the Raman spectra of the poled and unpoled sample at selected temperatures. We see that at room temperature, poled NBT exhibits relatively more symmetric mode as compared to the unpoled sample. In view of the structural results, the asymmetry in the unpoled sample can be attributed to excitation of additional vibrational modes around the local structural heterogeneities.[64] It is also interesting to note that this subtle difference in the profile of poled and unpoled samples exists only up to 200 °C [Fig. 9(b)], and above this temperature both show a similar pattern. This indicates that the major structural change in the poled sample occurs at the normal to relaxor ferroelectric transition. The whole spectra from 90 to 700 cm^{-1} were fit using four Lorentzian peaks by considering single peaks for region A and B and two peaks in region C. Since the peak in region A disappears above 300 °C, only three peaks were considered for fitting above this temperature. Figures 10(a) and 10(b) show the variation of the wavenumber of the modes in region A and B, respectively, for both poled and unpoled samples as a function of temperature. The anomalies in the modes of region C are not shown since the error associated is high due to the large line width and very diffuse peaks. Both the modes in region A and B show anomaly at 200 °C for the poled sample but not for the unpoled sample. This indicates sudden disturbance in the Na-O and Ti-O vibrations above $T_{F\text{-}R}$, signifying the onset of considerable local structural disorder in the system. This anomaly is not seen in the unpoled sample because the preexisting structural heterogeneities already present before $T_{F\text{-}R}$ mask the intrinsic instability. A similar situation was noted in the dielectric studies discussed previously [Fig. 8(b)]. Mode B shows another anomaly at 280 °C wherein the slope of the

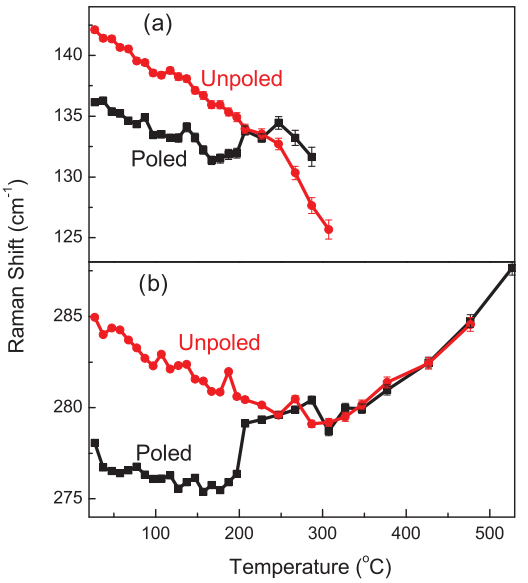

FIG. 10. (Color online) Variation of two modes of the Raman spectra with temperature for poled and unpoled NBT.

variation in the mode position suddenly changes [Fig. 10(b)]. This is accompanied by the mode in region A diffusing into the Rayleigh peak above this temperature. We assign this anomaly to the emergence of the tetragonal ($P4bm$) distortion in the sample, and this feature is common to both the poled and unpoled sample.

G. Structural transitions—x-ray and neutron diffraction studies

In order to corroborate the results of Raman analysis, temperature-dependent x-ray and neutron powder diffraction studies on poled specimen were carried out. As already pointed out, due to significant reduction in the structural heterogeneities, poled NBT exhibits well-defined and sharp Bragg peaks in the x-ray and neutron powder diffraction patterns, which can be fitted with a rhombohedral structural model. Since the dielectric study has revealed a sharp anomaly characteristic of a phase transition at 200 °C in the poled specimen, we anticipated detecting a drastic structural transition around the same temperature upon heating the poled specimen. The diffraction patterns were recorded by first heating the poled specimen and then cooling from the cubic phase. The data recorded during the cooling cycle can be considered as structural evolution of the unpoled NBT. Figures 11(a) and 11(b) show the evolution of the main Bragg peaks with temperature as contour plots. Both $\{110\}_c$ and $\{111\}_c$ peaks of the poled sample show drastic changes above $T_{F\text{-}R}$ (200 °C). The large split in the $\{111\}_c$ peak appears to suddenly collapse above this temperature. However the peak asymmetry survives until 280 °C. In contrast, the unpoled sample shows a smooth and continuous variation across 200 °C. A closer inspection of the shape of $\{111\}_c$ peak of poled NBT revealed that its peak shape at 210 °C is similar to that of the unpoled specimen at room temperature [Fig. 12(c)], which has been interpreted as monoclinic distortion.[29,45] Since the perceived average monoclinic distortion is due to the existence of localized in-phase tilted regions and the resulting heterogeneous lattice strain, the transition to the relaxor ferroelectric state on heating the poled sample above 200 °C must be due to a sudden increase in the structural heterogeneity in the field-stabilized $R3c$ matrix.

Additional information with regard to the temperature-induced structural changes was obtained by a neutron diffraction study of poled NBT by monitoring the evolution of the superlattice reflections. Data was collected by first heating and then cooling the powder of the poled specimen. The $\frac{1}{2}\{310\}_c$ superlattice reflection becomes discernible at 150 °C (Fig. 13). This corresponds to the same temperature above which sharp drop in the remnant polarization was noted earlier (Fig. 9). This proves that the onset of depoling is due to onset of the in-phase tilted octahedral regions in the poled specimen. At 200 °C, another superlattice reflection $\frac{1}{2}\{312\}_c$ becomes noticeable along with the $\frac{1}{2}\{310\}_c$ reflection. The intensity of these superlattice reflections increases abruptly in the narrow interval of 200–230 °C. Though conventionally these types of superlattice reflections have been associated with the tetragonal ($P4bm$) structure, the main Bragg profiles do not show any signature of tetragonal splitting below 280 °C in both x-ray and neutron diffraction patterns. The tetragonal splitting

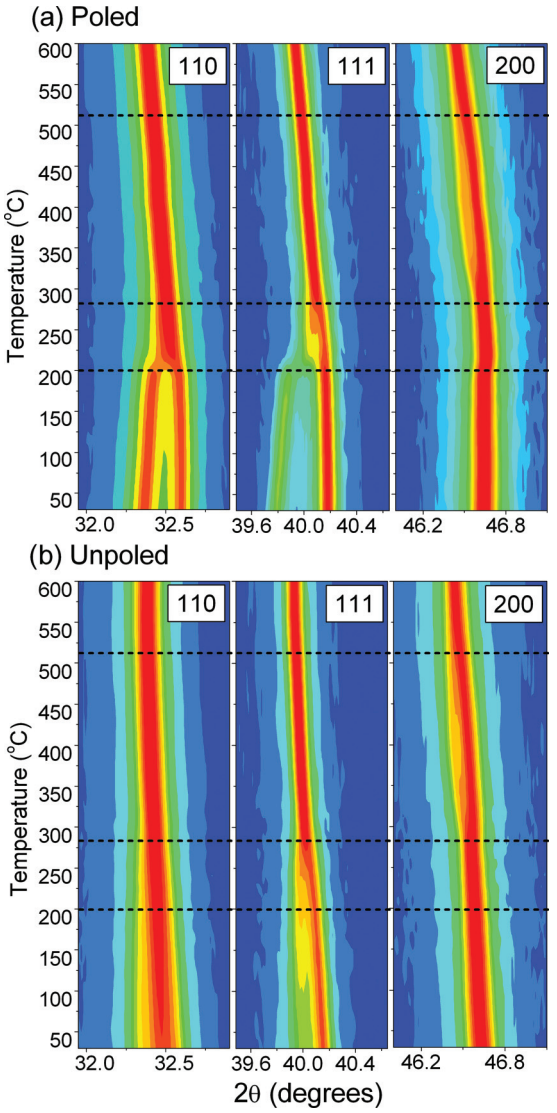

FIG. 11. (Color online) Contour plot of selected Bragg reflections of NBT obtained by high temperature XRD. The indexing of the Bragg reflections is done with respect to the pseudocubic cell. (a) Temperature dependence of initially poled NBT sample. (b) Temperature dependence of an unpoled NBT sample.

in the pseudocubic $\{200\}_c$ Bragg peak becomes noticeable only above 300 °C, which is well above the temperature at which $\frac{1}{2}\{ooe\}_c$ superlattice reflections begin to appear (150 °C). The emergence of spontaneous tetragonal strain manifests as a sudden increase in the full width half-maximum (FWHM) of the $\{200\}_c$ peak [Fig. 12(d)]. The odd-odd-odd superlattice reflection $\frac{1}{2}\{331\}_c$, which is characteristic of the $R3c/Cc$ phase, disappears at 300 °C (Fig. 13). Simultaneously, the FWHM of the $\{111\}_c$ XRD peak also becomes constant above 300 °C [Fig. 12(e)]. Both these features prove the complete disappearance of the $R3c$ phase above this temperature. The occurrence of both $\frac{1}{2}\{ooo\}$- and $\frac{1}{2}\{ooe\}$-type superlattice reflections in the temperature range 150–300 °C would seem to imply a coexistence of two phases, $P4bm$ and $R3c$. Figure 13 shows the Rietveld refinement fits of selected Bragg reflections of the neutron diffraction pattern at different temperatures with the $R3c + P4bm$ structural model. It is interesting to

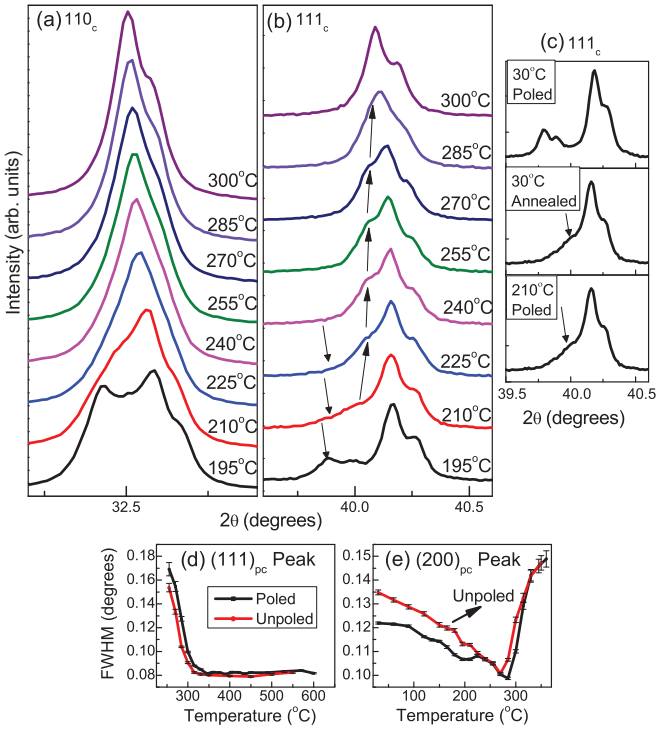

FIG. 12. (Color online) (a) Evolution of $\{110\}_c$ and (b) $\{111\}_c$ Bragg reflection as a function of temperature between 190 °C and 300 °C obtained from high temperature XRD. (c) Comparison of the $\{111\}_c$ peaks of the poled and unpoled samples at room temperature with that of the poled sample at 210 °C. The peak at 210 °C attains similar features as that of the unpoled sample. (d) Variation of the FWHM of the $\{111\}_c$ and (e) $\{200\}_c$ Bragg reflections as a function of temperature obtained from the XRD.

note that below 230 °C the intensities of the observed $\frac{1}{2}\{ooe\}$ superlattice reflections do not match with that predicted by the $P4bm$ model. This seems to indicate that the occurrence of the $\frac{1}{2}\{ooe\}_c$ superlattice reflections in the temperature range 150–230 °C may not correspond to a true $P4bm$ phase. We may also note that the intensities of these superlattice peaks could not be modeled by any of the other structural models in the Glazers scheme.[33,65] It is likely that this temperature range contains a modulated structure, as proposed by other groups.[24,32,42,43]

The entire XRD pattern at 300 °C mimics a cubiclike phase as all the peaks are singlet in nature. In fact, Rietveld refinement of the XRD pattern at 300 °C with a single phase cubic $Pm3m$ model yielded a very good fit (Fig. 14). However, this cannot actually be true since neutron diffraction patterns exhibit prominent $\frac{1}{2}\{ooe\}_c$-type superlattice peaks at this temperature. This particular temperature also corresponds to the temperature at which optical isotropization[28,38–40] has been reported in NBT single crystals. What is interesting to note is that not only are the Bragg peaks singlet but also that their FWHMs are very close to the FWHMs of the corresponding peaks when the specimen was in the high temperature cubic state (∼600 °C) at which no excess broadening is expected. For example, FWHM for $\{111\}_c$ and $\{200\}_c$ at 300 °C was 0.09° and 0.11°, respectively, whereas the widths in the cubic phase at 600 °C was found to be 0.08° and 0.10°,

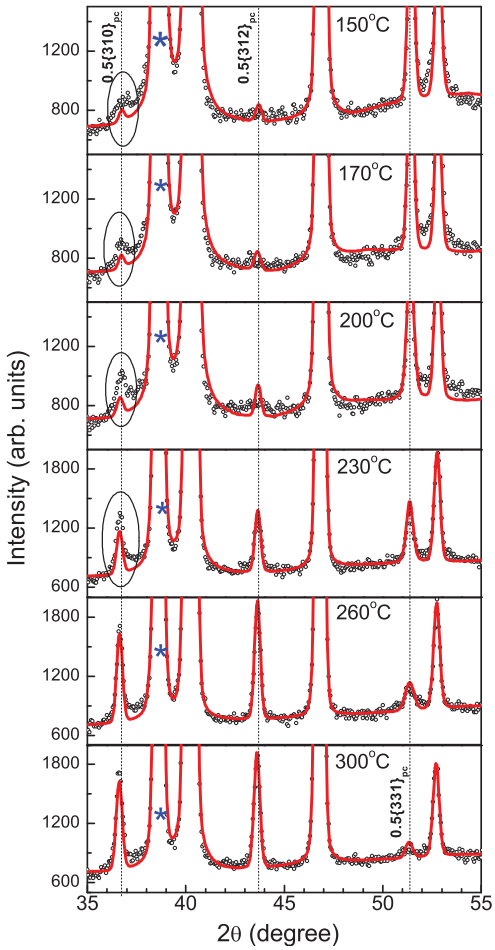

FIG. 13. (Color online) Rietveld refinement fits of selected angular range of the high temperature neutron diffraction data from 150 °C to 300 °C, fit using the $R3c + P4bm$ model. ∗ indicates the Niobium peak position originating from the container used. The encircled region shows the misfit between the observed and calculated Bragg profile.

respectively. A similar situation has been reported for 6 mol% $BaTiO_3$-substituted NBT at room temperature.[66,67] The phase at 300 °C is therefore a special type of noncubic structure with a cubiclike lattice parameter. This rules out the possibility of a

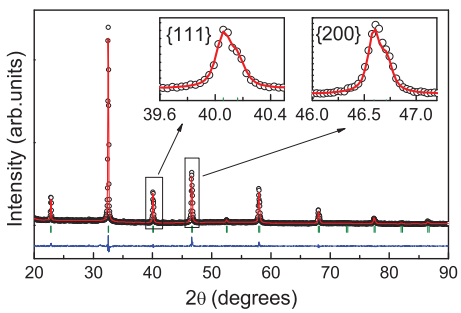

FIG. 14. (Color online) Rietveld refinement fit of high temperature XRD pattern of poled NBT at 300 °C with the cubic $Pm3m$ model. The refined cubic lattice parameter is 3.8951 (2) Å and the residual factor, $\chi^2 = 1.55$.

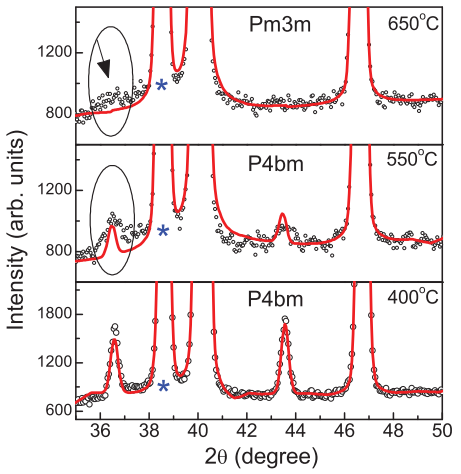

FIG. 15. (Color online) Rietveld refinement fits of selected angular range of the high temperature neutron diffraction data. (a) Pattern at 400 °C fit using the *P4bm* model. (b) Pattern at 550 °C fit using the *P4bm* model. (c) Pattern at 650 °C fit using the *Pm3m* model. ∗ indicates the Niobium peak position originating from the container used. The encircled region shows the misfit between the observed and calculated Bragg profile.

truly cubic optically isotropic structure at 300 °C, as speculated by Gorfman *et al.*[28] Also, it is less likely that the optical isotropization could be due to anomalously small domains with random orientations of the optical indicatrices, since for such a situation, one may expect considerable broadening of the XRD peaks, which is not the case. A more detailed experiment would be required to understand this phenomenon.

It is interesting to note that although the split between the pair of $\{h00\}_c$ reflections disappeared at 520 °C, signaling the tetragonal to cubic transformation (Fig. 11), the $\frac{1}{2}\{ooe\}_c$ superlattice peaks persisted beyond 520 °C (Fig. 15). The relative intensities of the superlattice reflections in the cubic phase region are similar to those observed in the temperature range 150–230 °C, which, as discussed above, could not be explained by the *P4bm* model. For example, as shown in Fig. 15, at 400 °C the pattern fits very well with the *P4bm* model whereas the pattern at 550 °C does not. This suggests that above 550 °C, the system may be treated with a coexistence of a cubic and a modulated structure consisting primarily of the in-phase tilted octahedra. This superlattice peak could be observed even up to 650 °C and confirms a similar observation made earlier by Trolliard and Dorcet,[43] who reported the superlattice reflections in their electron diffraction pattern at 620 °C. The occurrence of in-phase tilt components in the cubic phase suggests that NBT is prone to exhibit this kind of tilt disorder.

The above results can be summarized by the following.

High temperature XRD of poled NBT:

$$\mathrm{RT} \overset{R3c}{\Rightarrow} 200\,^{\circ}\mathrm{C} \overset{R3c/Cc}{\Rightarrow} 300\,^{\circ}\mathrm{C[cubic]} \overset{P4bm}{\Rightarrow} 520\,^{\circ}\mathrm{C} \overset{Pm3m}{\Rightarrow}$$

High temperature neutron diffraction of poled NBT:

$$\mathrm{RT} \overset{R3c}{\Rightarrow} 150\,^{\circ}\mathrm{C} \overset{1/2\{ooo\}+1/2\{ooe\}\mathrm{tilt}}{\Rightarrow} 230\,^{\circ}\mathrm{C} \overset{R3c/Cc+P4bm}{\Rightarrow}$$
$$300\,^{\circ}\mathrm{C} \overset{P4bm}{\Rightarrow} 520\,^{\circ}\mathrm{C} \overset{1/2\{ooe\}\mathrm{disorder}+Pm3m}{\Rightarrow}.$$

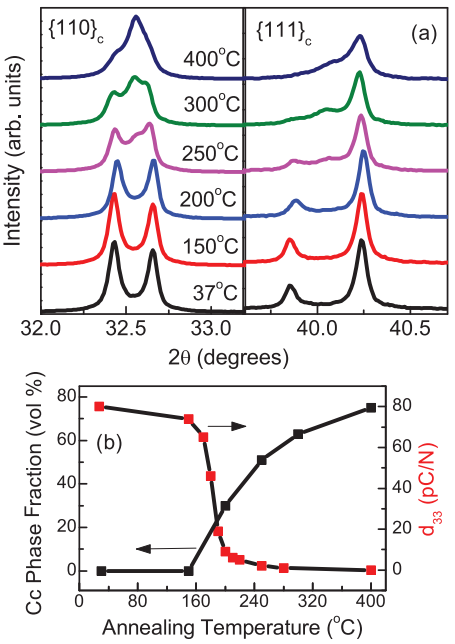

FIG. 16. (Color online) (a) Room temperature XRD plot of selected Bragg peaks of the poled NBT powder, which was annealed at different temperatures for 30 minutes and then cooled. The indexing of the peaks is done with respect to the pseudocubic cell. (b) Variation of volume fraction of the *Cc* phase for the poled NBT powder annealed at different temperatures, which was modeled with the $R3c + Cc$ model along with *ex situ* d_{33} measurement of poled NBT, which was annealed at different temperatures for 30 minutes.

H. Thermal aging of the poled specimen and structure-property correlation

Figure 16(a) shows the room temperature XRD plots of poled NBT powder, which has been heat treated to different temperatures. The diffraction pattern becomes similar to that of the unpoled sample only after heating the poled specimen above 300 °C, the optical isotropization temperature. Annealing the poled powder up to 200 °C does not cause any significant change in the room temperature pattern. In contrast, the room temperature pattern of poled powder that was annealed up to 250 °C shows peaks that are characteristic of both the unpoled and poled states. All the patterns in Fig. 16(a) could be refined with the $R3c + Cc$ structural model. As reported earlier,[37] the strategy of constrained refinement was adopted (lattice parameters and atomic coordinates fixed to that obtained for fully poled NBT and fully annealed NBT) to obtain a systematic variation in the fractions of the two phases. Figure 16(b) shows the variation of the *Cc* phase with increasing annealing temperature obtained from the Rietveld analysis along with the variation of d_{33}. It is interesting to note that though the d_{33} decreases considerably at 200 °C, it becomes zero only after annealing above 300 °C, thereby confirming that in spite of considerable depolarization beyond 200 °C, the system retains to some extent the memory of the poled state up to this temperature.

IV. DISCUSSION

A. The relaxor/normal ferroelectric dilemma

The relaxor behavior in the lead-based ferroelectric compounds $Pb(Mg_{1/3}Nb_{2/3})O_3$ (PMN), $Pb(Zn_{1/3}Nb_{2/3})O_3$ (PZN), $Pb(Sc_{1/2}Ta_{1/2})O_3$ (PST), and La-modified $Pb(Zr_{1-x}Ti_x)O_3$ (PLZT) are generally attributed to presence of polar nanoregions (PNRs), the correlation length of which grows on cooling from the high temperature cubic phase. Can NBT be categorized in the same way? There are several contrasting features that make NBT somewhat different from the canonical relaxor ferroelectrics such as PMN. For example, while the canonical systems exhibit (i) very insignificant lattice distortion below the dipolar freezing temperature, (ii) slim polarization hysteresis loop, and (iii) frequency-dependent dielectric maximum temperature in permittivity temperature plots, NBT exhibits a well-defined saturated polarization hysteresis loop, significant rhombohedral/monoclinic lattice distortion with respect to the paraelectric cubic structure and most interestingly a dielectric maximum temperature at ∼320 °C, which is not frequency dependent. These features are rather representative of a normal ferroelectric material such as $BaTiO_3$, $PbTiO_3$, or $KNbO_3$. However, in contrast to the normal ferroelectrics, polarization in NBT does not develop below the permittivity maximum ∼320 °C but only below ∼200 °C. Around this temperature, NBT exhibits a weak shoulder in the real part of the temperature-dependent permittivity and frequency-dependent peaks in the imaginary part. Earlier structural studies carried out on unpoled NBT specimens were unable to identify any anomalies around the depolarization temperature (200 °C). This is analogous to what is commonly observed in lead-based relaxors,[56,68] thereby prompting NBT to be categorized as a relaxor ferroelectric and not a normal ferroelectric. Petzelt *et al.*,[59] using dielectric, infrared, and Raman spectroscopy, discussed the dynamic aspects of the nanoregions in NBT and showed that the critical dynamics of these regions lie in the 5–10 GHz range. Unlike usual relaxors, they indicate that the characteristic relaxor behavior appears only in the gigahertz range in NBT; hence, standard dielectric measurements at a lower frequency will not show any major dispersion. Lattice dynamical studies, on the other hand, have shown similarity between NBT and PMN in terms of the occurrence of overdamped soft modes, a "waterfall" effect, and its disappearance below the depolarization temperature.[69] Analogous to PMN, it might be tempting to attribute the dielectric relaxation below the depolarization temperature to the PNRs centered around the nanosized planar defects.[25,32] Kreisel *et al.* have argued about the difference in the nature of the PNRs in NBT and PMN by highlighting the remarkable asymmetric diffuse scattering in NBT against the symmetric diffuse scattering in PMN.[70] This particular difference at room temperature may be due to the comparatively smaller size of the PNRs in PMN since the freezing temperature of the PNRs is below room temperature in PMN as compared to ∼190 °C in NBT. A better appreciation of the difference in signatures of the diffuse scattering would require a temperature-dependent diffuse x-ray scattering study. TEM studies have offered enough evidence to suggest that nanoregions that give rise to diffuse scattering are in low volume fraction and too small to be detected in bulk diffraction experiments (x-ray and neutron). However, they are sufficiently big enough to show coherent diffraction and reveal the localized in-phase octahedral tilt (1–3 nm). The localized structural and strain heterogeneities would break the long-range polar order and make the system mimic as a relaxor ferroelectric. The considerable dielectric relaxation and absence of visible structural change at 200 °C in the unpoled specimen is akin to the nonergodic relaxor state of NBT at room temperature. Poling of NBT at room temperature transforms it irreversibly to a ferroelectric state as evident from the drastic reduction in dielectric dispersion, appearance of well-defined polarization-electric field hysteresis loop and establishment of a homogeneous $R3c$ distortion.

B. Status of the reported global monoclinic phase

Monoclinic structures are of great interest in ferroelectric solid solutions exhibiting morphotropic phase boundary (MPB) as they are considered to be responsible for the high piezoelectric response by providing a low energy pathway for continuous rotation of the polarization vector on application of external field.[71] So far, such structures have been encountered mostly in ferroelectric solid solutions[72] and not in pure compounds, though such a possibility has been predicted for $PbTiO_3$ at high pressure and low temperature.[73] Ever since the report of the average monoclinic distortion in NBT, the status of this phase remained unclear. Initially, the monoclinic distortion was proposed on a very local scale to explain the diffuse x-ray scattering. It was suggested that Na/Bi are displaced along the $\langle 100\rangle_c$ direction away from the $\langle 111\rangle_c$ to yield a localized monoclinic distortion.[25] Electron diffraction studies on the other hand reported localized in-phase tilted octahedral regions. The two techniques seem to reveal different aspects of the same local structural distortion. The most notable result in recent years is the claim of global monoclinic distortion in NBT. Gorfman *et al.*[28] have supported the global monoclinic distortion in their recent optical birefringence study of NBT crystals as they failed to observe well-defined domain walls, expected for the rhombohedral symmetry. This negative result, however, cannot be treated as a conclusive evidence for monoclinic symmetry. Earlier, Geday *et al.*[38] interpreted the lack of well-defined domain walls in their birefringence study to the existence of twinning coupled with strain, in conformity with the high level of strain reported earlier by Isupov and Kurzina.[74] The lack of long-range coherence in the HRTEM (Fig. 5) images supports the strain-induced randomization of optical birefringence. Another important question that needs to be answered is whether the monoclinic distortion in NBT corresponds to a thermodynamically equilibrium state as in the conventional MPB systems? It may be remarked that compared to the lead-based MPB systems, the piezoelectric response of NBT is significantly low (d_{33} ∼ 80 pC/N). In fact it requires substitution of about 6 mol% Ba to increase its piezoelectric coefficient.[3] If the monoclinic distortion in NBT represents an equilibrium state, then why should the electric field permanently destroy this state and convert it to rhombohedral? One would rather anticipate the equilibrium state to revert back to a great extent after the field is switched off, as has recently been demonstrated in $PbTiO_3$-$BiScO_3$.[75]

With regard to the average monoclinic distortion reported in high resolution XRD based studies, there can be two possible scenarios. In view of the fact that the TEM studies have shown the presence of fine scale pseudorhombohedral twin domains that reside preferentially on {100} planes,[32] the explanation for the monocliniclike distortion in high resolution global diffraction experiments may be sought within the framework of the adaptive phase model.[76] According to this theory, the monocliniclike diffraction pattern can appear due to adaptive coherent scattering from nanosized rhombohedral domains.[36] Though the details are yet to be fully understood, a plausible reason for the formation of nanosized rhombohedral domains in NBT may be attributed to the compulsion for the $R3c$ regions to grow within the complex domain patterns set by the high temperature $P4bm$ phase. Application of the electric field seems to merge the rhombohedral nanodomains and increase its coherence length. Further, since the nanosized rhombohedral domain state is not a thermodynamic compulsion at room temperature, there is no competing factor that could force the system to revert back to the nanodomain state after removal of the field. In the absence of the adaptive coherent scattering, the diffraction experiments would reveal the true symmetry of the structure. This field-stabilized long-range coherence of the rhombohedral lattice is substantially disturbed only after the in-phase tilt regions grow significantly when heated beyond 200 °C. The second possibility is that the strain due to the incompatible in-phase tilt distorts the rhombohedral matrix to actually make it monoclinic on a mesoscopic length scale around itself. In this scenario, the strain would not be uniform throughout the matrix; hence, the amount of distortion would vary in different regions. This would lead to a monoclinic distortion with a distribution of cell parameters that cannot be modeled with a single phase. Application of the electric field in this case would minimize the in-phase tilted regions and thereby also remove the strain on the matrix. Global diffraction techniques will then be able to reveal the actual rhombohedral $R3c$ structure. In view of the results presented in this paper, it is anticipated that poling would drastically reduce the x-ray and neutron diffuse scattering signal[24,25] and also reduce the extent of random orientation of indicatrices in an optical birefringence study.[28]

C. Depoling and structural changes

Though the depolarization temperature at ∼200 °C is well known for NBT, structural studies on unpoled specimens have failed to offer any insight with regard to the nature of the structural changes around this temperature. In fact, as noted above, the lack of structural anomaly around 200 °C has been taken as evidence in support of the relaxor ferroelectric character of NBT. Since the perceived average structure changes from monoclinic to rhombohedral on application of the high electric field,[36] looking for a correlation between the depolarization behavior of NBT and temperature-induced structural changes in unpoled specimen was, perhaps, not the right strategy. The present study reveals that the depolarization is associated with the onset of incompatible in-phase tilt in the field stabilized homogeneous $R3c$ matrix. This phenomenon starts at approximately 50 °C below the reported depolarization temperature (∼200 °C). The field-stabilized homogeneous $R3c$ lattice is not disturbed until 200 °C. Near the depolarization temperature, the long-range coherence of the rhombohedral lattice decreases drastically due to the sudden increase in the in-phase tilted regions. The fraction of the monocliniclike distortion, which is indicative of permanent precipitation of nanosized structural heterogeneity in the rhombohedral lattice, increases with an increasing annealing temperature in the 200–300 °C range. Partial restoration of the field-stabilized rhombohedral distortion was not possible any more after heating the poled specimen above 300 °C, the optical isotropization temperature. That the system could retain some memory of the field-stabilized distortion after cooling from a maximum temperature of 300 °C suggests that it is not completely paraelectric up to this temperature.

D. Tilt disorder—an intrinsic feature in NBT

The origin of the complicated dielectric, ferroelectric, and structural phase transition behavior of NBT lies in the disorder of the Na^{1+} and Bi^{3+} ions on the A-site of the ABO_3 perovskite and the contrasting nature of Na-O and Bi-O bonds. While the Na-O bond is ionic, the Bi-O bond is highly covalent due to the lone pair $6s^2$ of the Bi^{3+}. Bond-valence calculations by Jones and Thomas[23] showed that Bi was severely under bonded when the average rhombohedral $R3c$ structure of NBT was considered. Even the XAFS study by Shuvaeva *et al.*[26] showed that the local environment of Bi is heavily distorted, and the shortest Bi-O bond distance was found to be 2.22 Å, which is 0.3 Å shorter than that calculated from crystallographic data. The random occupancy of Na and Bi in conjunction with the severe contrast in the bonding characteristics of Na and Bi with O is expected to bring about positional disorder on the oxygen sublattice. The presence of localized in-phase octahedral tilt even in the global cubic phase[43] (Fig. 15), seems to be a manifestation of this intrinsic oxygen positional disorder. The slow decrease in the intensity of the superlattice reflections on heating in the global cubic state suggests that the in-phase tilted octahedral regions may survive at a localized scale well above the temperature at which these superlattice reflections become invisible in the neutron diffraction. The complex phase transition behavior of NBT can therefore be considered as a result of the intrinsic lattice instabilities in the midst of the ever-present in-phase tilt disorder. While this in-phase tilt disorder is compatible with the tetragonal $P4bm$ distortion, it is incompatible with the $R3c$ ferroelectric distortion. The local monoclinic displacement of A-site cations within the disk-shaped structural heterogeneity found in the local structure analysis[25] appears to be a result of competing displacement tendencies in the global $R3c$ and the local $P4bm$ regions. The simultaneous vanishing of (i) local in-phase tilted regions, (ii) strain heterogeneity, and (iii) the monocliniclike average lattice distortion suggests that the poling field is able to force Bi, Na, and O to irreversibly take up positions compatible with the global $R3c$ phase. It appears that though local factors did not allow the system to stabilize in its equilibrium $R3c$ structure, electric field helps in acquiring that very state by suppressing the local structural heterogeneity. Ferroelectric distortion in Bi-perovskite-based ferroelectric systems such as $BiAlO_3$ (Ref. 77) and $BiFeO_3$ (Ref. 78) are primarily stabilized by the highly covalent character of the Bi-O bonds because

of the $6s^2$ lone pair electrons of Bi^{3+}. Though 50% of the A-site is replaced by ferroelectrically inactive Na in NBT, the reinforcement in favor of the $R3c$ ferroelectric distortion seems to come from the Ti-O hybridization as in $BaTiO_3$ (Ref. 79).

V. CONCLUSIONS

In this work, a self-consistent set of mutually complementing experimental and first-principles techniques were used to resolve the interrelationship between (i) local structural heterogeneities, (ii) the recently suggested average monoclinic (Cc) structure, and (iii) its influence on the dielectric and ferroelectric behavior of the lead-free $Na_{0.5}Bi_{0.5}TiO_3$. First-principles study in conjunction with electric field-dependent electron, neutron, and XRD study confirmed the global rhombohedral ($R3c$) phase to be more stable than the monoclinic (Cc) phase. The monocliniclike distortion observed in bulk diffraction techniques was found to be a result of the strain generated by the localized in-phase (+) tilted octahedral regions in the $R3c$ matrix. Electric poling drastically reduces the coherence length of the localized in-phase tilt and also the strain heterogeneities in the average lattice, thereby enabling the ground state $R3c$ structure of NBT to be revealed on a global length scale. The disorder/strain-free system exhibits anomalous structural instability at $T_{F\text{-}R}$ while heating, a feature that has not been possible to capture in the unpoled specimen due to its masking by the preexisting structural heterogeneity. A one-to-one correlation between the onset of depoling (∼150 °C) and appearance of in-phase tilted octahedral regions has been established. The depolarization temperature is marked by the critical increase in the in-phase tilted octahedral region. At around 300 °C, the reported optical isotropization temperature, NBT exhibits a special noncubic structure with a cubiclike lattice parameter. Interestingly, though the depolarization seems to be complete at ∼200 °C, the system retains some memory of the field-stabilized $R3c$ phase until 300 °C, suggesting sustenance of weak polarization up to this temperature. The results suggest the prominent role of in-phase (+) tilted octahedral disorder in influencing the dielectric, ferroelectric, and piezoelectric properties of NBT. This disorder is intrinsic to the system and is associated with the contrasting characteristics of Na-O and Bi-O bonds, which tend to create positional disorder on the oxygen sublattice and manifest as localized in-phase tilted octahedral regions. In the zero field state the intrinsic lattice instabilities (ferroelectric or otherwise) in NBT therefore occur in the midst of this ever-present tilt disorder. The understanding acquired in this study will provide the framework for understanding the structure-property correlations of the substituted NBT systems, which are promising candidates as lead-free piezoelectric alternatives.

ACKNOWLEDGMENTS

RR gratefully acknowledges financial assistance from Department of Science and Technology (DST) and the Council of Scientific and Industrial Research (CSIR), India.

*Corresponding author: rajeev@materials.iisc.ernet.in

[1] G. A. Smolenskii, V. A. Isupv, A. I. Afranovskaya, and N. N. Kainik, J. Solid State Phys. **11**, 2651 (1961).
[2] S.-T. Zhang, A. B. Kounga, E. Aulbach, T. Granzow, W. Jo, H.-J. Kleebe, and J. Rödel, J. Appl. Phys. **103**, 034107 (2008).
[3] T. Takenaka, K. Maruyama, and K. Sakata, Jpn. J. Appl. Phys. **30**, 2236 (1991).
[4] T. Takenaka and H. Nagata, J. Eur. Ceram. Soc. **25**, 2693 (2005).
[5] W. Jo, R. Dittmer, M. Acosta, J. Zang, C. Groh, E. Sapper, K. Wang, and J. Rödel, J. Electroceram. **29**, 71 (2012).
[6] T. Takenaka, H. Nagata, and Y. Hiruma, Jpn. J. Appl. Phys. **47**, 3787 (2008).
[7] J. Rödel, W. Jo, K. T. P. Seifert, E.-M. Anton, T. Granzow, and D. Damjanovic, J. Am. Ceram. Soc. **92**, 1153 (2009).
[8] R. Dittmer, W. Jo, D. Damjanovic, and J. Rödel, J. Appl. Phys. **109**, 034107 (2011).
[9] Y.-M. Chiang, G. W. Farrey, and A. N. Soukhojak, Appl. Phys. Lett. **73**, 3683 (1998).
[10] Y. Hosono, K. Harada, and Y. Yamashita, Jpn. J. Appl. Phys. **40**, 5722 (2001).
[11] K. G. Webber, Y. Zhang, W. Jo, J. E. Daniels, and J. Rödel, J. Appl. Phys. **108**, 014101 (2010).
[12] O. Elkechai, M. Manier, and J. P. Mercurio, Phys. Status Solidi A **157**, 499 (1996).
[13] A. Sasaki, T. Chiba, Y. Mamiya, and E. Otsuki, Jpn. J. Appl. Phys. **38**, 5564 (1999).
[14] V. A. Isupov, Ferroelectrics **315**, 123 (2005).
[15] B. Wylie-van Eerd, D. Damjanovic, N. Klein, N. Setter, and J. Trodahl, Phys. Rev. B **82**, 104112 (2010).
[16] F. Cordero, F. Craciun, F. Trequattrini, E. Mercadelli, and C. Galassi, Phys. Rev. B **81**, 144124 (2010).
[17] C. Ma, X. Tan, E. Dul'kin, and M. Roth, J. Appl. Phys. **108**, 104105 (2010).
[18] J. E. Daniels, W. Jo, J. Rödel, and J. L. Jones, Appl. Phys. Lett. **95**, 032904 (2009).
[19] W. Jo, J. E. Daniels, J. L. Jones, X. Tan, P. A. Thomas, D. Damjanovic, and J. Rödel, J. Appl. Phys. **109**, 014110 (2011).
[20] J. Kreisel, A. M. Glazer, G. Jones, P. A. Thomas, L. Abello, and G. Lucazeau, J. Phys.: Condens. Matter **12**, 3267 (2000).
[21] K. T. P. Seifert, W. Jo, and J. Rödel, J. Am. Ceram. Soc. **93**, 1392 (2010).
[22] R. Dittmer, E. Aulbach, W. Jo, K. G. Webber, and J. Rödel, Scr. Mater. **67**, 100 (2012).
[23] G. O. Jones and P. A. Thomas, Acta Crystallogr. B **58**, 168 (2002).
[24] A. M. Balagurov, E. Y. Koroleva, A. A. Naberezhnov, V. P. Sakhnenko, B. N. Savenko, N. V. Ter-Oganessian, and S. B. Vakhrushev, Phase Transit. **79**, 163 (2006).
[25] J. Kreisel, P. Bouvier, B. Dkhil, P. A. Thomas, A. M. Glazer, T. R. Welberry, B. Chaabane, and M. Mezouar, Phys. Rev. B **68**, 014113 (2003).
[26] V. A. Shuvaeva, D. Zekria, A. M. Glazer, Q. Jiang, S. M. Weber, P. Bhattacharya, and P. A. Thomas, Phys. Rev. B **71**, 174114 (2005).

[27]S. Gorfman and P. A. Thomas, J. Appl. Crystallogr. **43**, 1409 (2010).
[28]S. Gorfman, A. M. Glazer, Y. Noguchi, M. Miyayama, H. Luo, and P. A. Thomas, J. Appl. Crystallogr. **45**, 444 (2012).
[29]E. Aksel, J. S. Forrester, J. L. Jones, P. A. Thomas, K. Page, and M. R. Suchomel, Appl. Phys. Lett. **98**, 152901 (2011).
[30]V. Dorcet and G. Trolliard, Acta Mater. **56**, 1753 (2008).
[31]R. Beanland and P. A. Thomas, Scr. Mater. **65**, 440 (2011).
[32]I. Levin and I. M. Reaney, Adv. Funct. Mater. **22**, 3445 (2012).
[33]A. M. Glazer, Acta Crystallogr. B **28**, 3384 (1972).
[34]A. M. Glazer, Acta Crystallogr. Sect. A **31**, 756 (1975).
[35]C. Ma, H. Guo, and X. Tan, Adv. Funct. Mater. **23**, 5261 (2013).
[36]B. N. Rao and R. Ranjan, Phys. Rev. B **86**, 134103 (2012).
[37]B. N. Rao, A. N. Fitch, and R. Ranjan, Phys. Rev. B **87**, 060102 (2013).
[38]M. Geday, J. Kreisel, A. M. Glazer, and K. Roleder, J. Appl. Crystallogr. **33**, 909 (2000).
[39]T. V. Kruzina, V. V. Gene, V. A. Isupov, and E. V. Sinyakov, Sov. Phys. Crystallogr. **26**, 852 (1981).
[40]S.-E. Park, S.-J. Chung, I.-T. Kim, and K. S. Hong, J. Am. Ceram. Soc. **77**, 2641 (1994).
[41]Y. Hiruma, H. Nagata, and T. Takenaka, J. Appl. Phys. **105**, 084112 (2009).
[42]V. Dorcet, G. Trolliard, and P. Boullay, Chem. Mater. **20**, 5061 (2008).
[43]G. Trolliard and V. Dorcet, Chem. Mater. **20**, 5074 (2008).
[44]V. Dorcet, G. Trolliard, and P. Boullay, J. Magn. Magn. Mater. **321**, 1758 (2009).
[45]E. Aksel, J. S. Forrester, B. Kowalski, J. L. Jones, and P. A. Thomas, Appl. Phys. Lett. **99**, 222901 (2011).
[46]D. S. Keeble, E. R. Barney, D. A. Keen, M. G. Tucker, J. Kreisel, and P. A. Thomas, Adv. Funct. Mater. **23**, 185 (2013).
[47]M. Hoelzel, A. Senyshyn, N. Juenke, H. Boysen, W. Schmahl, and H. Fuess, Nucl. Instrum. Methods Phys. Res. Sect. Accel. Spectrometers Detect. Assoc. Equip. **667**, 32 (2012).
[48]J. R. Carvajal, *FULLPROF. A Rietveld Refinement and Pattern Matching Analysis Program* (Laboratoire Leon Brillouin, CEA-CNRS, France, 2000).
[49]G. Kresse and J. Hafner, Phys. Rev. B **47**, 558 (1993).
[50]P. E. Blöchl, Phys. Rev. B **50**, 17953 (1994).
[51]J. P. Perdew, K. Burke, and Y. Wang, Phys. Rev. B **54**, 16533 (1996).
[52]C. Ma, H. Guo, S. P. Beckman, and X. Tan, Phys. Rev. Lett. **109**, 107602 (2012).
[53]M. K. Niranjan, T. Karthik, S. Asthana, J. Pan, and U. V. Waghmare, J. Appl. Phys. **113**, 194106 (2013).
[54]S. B. Vakhrushev, V. A. Isupov, B. E. Kvyatkovsky, N. M. Okuneva, I. P. Pronin, G. A. Smolensky, and P. P. Syrnikov, Ferroelectrics **63**, 153 (1985).
[55]P. A. Thomas, S. Trujillo, M. Boudard, S. Gorfman, and J. Kreisel, Solid State Sci. **12**, 311 (2010).
[56]D. Viehland, S. J. Jang, L. E. Cross, and M. Wuttig, J. Appl. Phys. **68**, 2916 (1990).
[57]A. E. Glazounov and A. K. Tagantsev, Appl. Phys. Lett. **73**, 856 (1998).
[58]W. Jo, J. Daniels, D. Damjanovic, W. Kleemann, and J. Rödel, Appl. Phys. Lett. **102**, 192903 (2013).
[59]J. Petzelt, S. Kamba, J. Fábry, D. Noujni, V. Porokhonskyy, A. Pashkin, I. Franke, K. Roleder, J. Suchanicz, R. Klein, and G. E. Kugel, J. Phys.: Condens. Matter **16**, 2719 (2004).
[60]I. G. Siny, E. Husson, J. M. Beny, S. G. Lushnikov, E. A. Rogacheva, and P. P. Syrnikov, Ferroelectrics **248**, 57 (2000).
[61]B. K. Barick, K. K. Mishra, A. K. Arora, R. N. P. Choudhary, and D. K. Pradhan, J. Phys. Appl. Phys. **44**, 355402 (2011).
[62]L. Luo, W. Ge, J. Li, D. Viehland, C. Farley, R. Bodnar, Q. Zhang, and H. Luo, J. Appl. Phys. **109**, 113507 (2011).
[63]J. Kreisel, A. M. Glazer, P. Bouvier, and G. Lucazeau, Phys. Rev. B **63**, 174106 (2001).
[64]C. M. Foster, M. Grimsditch, Z. Li, and V. G. Karpov, Phys. Rev. Lett. **71**, 1258 (1993).
[65]H. T. Stokes, E. H. Kisi, D. M. Hatch, and C. J. Howard, Acta Crystallogr. B **58**, 934 (2002).
[66]R. Garg, B. N. Rao, A. Senyshyn, P. S. R. Krishna, and R. Ranjan, Phys. Rev. B **88**, 014103 (2013).
[67]R. Ranjan and A. Dviwedi, Solid State Commun. **135**, 394 (2005).
[68]G. Burns and F. H. Dacol, Solid State Commun. **48**, 853 (1983).
[69]M. Matsuura, H. Iida, K. Hirota, K. Ohwada, Y. Noguchi, and M. Miyayama, Phys. Rev. B **87**, 064109 (2013).
[70]J. Kreisel, P. Bouvier, B. Dkhil, B. Chaabane, A. M. Glazer, P. A. Thomas, and T. R. Welberry, Ferroelectrics **302**, 293 (2004).
[71]H. Fu and R. E. Cohen, Nature **403**, 281 (2000).
[72]B. Noheda, Curr. Opin. Solid State Mater. Sci. **6**, 27 (2002).
[73]Z. Wu and R. E. Cohen, Phys. Rev. Lett. **95**, 037601 (2005).
[74]V. A. Isupov and T. V. Kurzina, Izv. AN SSSR, Ser. Fiz. **47**, 616 (1983) [Sov. Phys.: Bull. Acad. Sci. USSR, Phys. Ser. **47**, 194 (1983)].
[75]K. V. Lalitha, A. N. Fitch, and R. Ranjan, Phys. Rev. B **87**, 064106 (2013).
[76]Y. U. Wang, Phys. Rev. B **76**, 024108 (2007).
[77]P. Baettig, C. F. Schelle, R. LeSar, U. V. Waghmare, and N. A. Spaldin, Chem. Mater. **17**, 1376 (2005).
[78]F. Kubel and H. Schmid, Acta Crystallogr. B **46**, 698 (1990).
[79]R. E. Cohen, Nature **358**, 136 (1992).